Slow Cooperative Folding of a Small Globular Protein HPr†

Nico A. J. Van Nuland,[‡,§] Wim Meijberg,[§] Jessica Warner,[§] Vincent Forge,[‡,||] Ruud M. Scheek,[§] George T. Robillard,[§] and Christopher M. Dobson*[,‡]

New Chemistry Laboratory, Oxford Centre for Molecular Sciences, University of Oxford, South Parks Road, Oxford OX1 3QT, U.K., and Groningen Biomolecular Sciences and Biotechnology Institute, University of Groningen, Nijenborgh 4, 9747 AG Groningen, The Netherlands

Received July 23, 1997; Revised Manuscript Received October 22, 1997[⊗]

ABSTRACT: The folding of an 85-residue protein, the histidine-containing phosphocarrier protein HPr, has been studied using a variety of techniques including DSC, CD, ANS fluorescence, and NMR spectroscopy. In both kinetic and equilibrium experiments the unfolding of HPr can be adequately described as a two-state process which does not involve the accumulation of intermediates. Thermodynamic characterization of the native and the transition states has been achieved from both equilibrium and kinetic experiments. The heat capacity change from the denatured state to the transition state (3.2 kJ mol^{-1} K^{-1}) is half of the heat capacity difference between the native and denatured states (6.3 kJ mol^{-1} K^{-1}), while the solvent accessibility of the transition state (0.36) indicates that its compactness is closer to that of the native than that of the denatured state. The high value for the change in heat capacity upon unfolding results in the observation of cold denaturation at moderate denaturant concentrations. Refolding from high denaturant concentrations is, however, slow. The rate constant of folding in water, $k_f^{H_2O}$ (14.9 s^{-1}), is small compared to that reported for other proteins of similar size under similar conditions. This indicates that very fast refolding is not a universal character of small globular proteins which fold in the absence of detectable intermediates.

In view of the enormous number of tertiary folds that are conceivable for a small protein, it is remarkable that a given protein shows such a strong preference for a single structure. The information directing the protein to its native state is encoded in its amino acid sequence, but the nature of this information is not yet well understood (see 1 and references therein). For a full understanding of the physical interactions that stabilize a protein in a given fold, a detailed description of its stability in terms of the free energy of unfolding is vital. The stability of a protein is often estimated from an analysis of denaturant-induced or thermally induced unfolding transitions, measured either spectroscopically or calorimetrically. Here we present the results from unfolding of the histidine-containing phosphocarrier protein (HPr),[1] a small monomeric protein, by guanidine hydrochloride (GdnHCl) and by heat using differential scanning calorimetry (DSC), circular dichroism (CD), and fluorescence as well as nuclear magnetic resonance (NMR) spectroscopy. CD and fluorescence are well-established spectroscopic techniques that have been extensively used to study both equilibrium and kinetic details of the folding and unfolding processes of a large range of proteins (*2*). NMR has recently been applied to study the refolding process from high concentrations of denaturant in real time by the recording of a series of one-dimensional (1D) spectra (*3, 4*) and by directly following the refolding process during the recording of a single two-dimensional (2D) spectrum (*5*).

An essential step in the transport of carbohydrates across the cell membrane of bacteria via the phospho(enol)pyruvate-dependent sugar phosphotransferase system (PTS) involves the transfer of a phosphoryl-group from enzyme I to HPr and its subsequent donation to enzyme II, the membrane-bound transporter (*6*). The structural features of HPr's from different species have been extensively studied by both NMR spectroscopy (*7*−*11*) and X-ray diffraction (*12*−*14*). HPr shows a classical open-face β-sandwich fold consisting of three α-helices packed against a four-stranded antiparallel β-sheet. HPr from *Escherichia coli* consists of 85 amino acid residues. It lacks cysteine, tryptophan, and tyrosine but has a large number of leucine residues and four phenylalanines. Two proline residues, Pro11 and Pro18, both of which are in a *trans* configuration are positioned on either side of the active site residue His15, in two distinct structural elements; Pro11 is at position 3 in a type I′ turn and Pro18 at the N+2 position in the first α-helix. The fold of HPr

† N.A.J.v.N. and V.F. were supported by the Human Capital and Mobility Programme of the European Community. This work is a contribution from the Oxford Centre for Molecular Sciences which is supported by EPSRC, BBSRC, and MRC. The research of C.M.D. is supported in part by an International Research Scholars award from the Howard Hughes Medical Institute.

* Corresponding author. Tel.: +44-(0)1865-275916. Fax: +44-(0)-1865−275921. E-mail: chris.dobson@chem.ox.ac.uk.

‡ University of Oxford.

§ University of Groningen.

|| Present address: CNRS, URA 2096; SBPM, DBCM, CEA-CE Saclay, 91191 Gif-sur-Yvette, France.

⊗ Abstract published in *Advance ACS Abstracts,* December 1, 1997.

[1] Abbreviations: ANS, 8-anilino-1-naphthalenesulfonic acid; CD, circular dichroism; DSC, differential scanning calorimetry; GdnHCl, guanidine hydrochloride; HPr, histidine-containing phosphocarrier protein; PTS, the phospho(enol)pyruvate-dependent sugar phosphotransferase system.

S0006-2960(97)01794-7 CCC: $15.00
Published on Web 01/13/1998

has been related to that of several other proteins including ferredoxin, the RNA binding domains of ribonucleoprotein A and C, the activation domain of procarboxypeptidase B, acylphosphatase, and nucleoside diphosphate kinase (*15*−*17*).

As a result of the lack of tryptophan and tyrosine residues, the spectroscopic probes available for folding studies on wild type HPr are limited. Nevertheless, CD in the far- and near-ultraviolet (UV), and fluorescence associated with the binding of 8-anilino-1-naphthalenesulfonic acid (ANS) have been combined with NMR spectroscopy and DSC to study equilibrium and kinetic features of the folding and unfolding. From both kinetic and equilibrium studies, it is evident that the unfolding of HPr can be adequately described as a two-state process without the accumulation of intermediates, a common feature observed for proteins smaller than 100 residues (*18*). In contrast, the refolding from high denaturant concentrations is rather slow, indicating that fast folding in the absence of intermediates for these small proteins is not a general rule. Recently, the stability of HPr from *Bacillus subtilis* (*19*) and of *E. coli* (*20*) have been obtained from CD studies using urea as denaturant. Here we discuss differences and similarities between these studies and our findings using GdnHCl as denaturant.

MATERIALS AND METHODS

The production and purification of uniformly ^{15}N-enriched HPr has been described previously (*21*). For the production of unlabeled HPr, Luria-Bertani medium was used instead of mineral medium. All experiments were carried out using HPr buffered in a solution of 10 or 100 mM sodium or potassium phosphate (NaP_i/KP_i) at pH 7.6 or 7.0. The concentrations of GdnHCl were checked by refractive index measurements as described by Pace (*22*). For all DSC experiments, concentrations of HPr were determined by quantitative amino acid analysis. For all other experiments, the HPr concentration was measured by UV absorption at 259 nm using a Perkin Elmer Lambda 2S spectrometer using a extinction coefficient of 1900 M^{-1} cm^{-1}.

High-performance liquid chromatography (HPLC) experiments were carried out to determine the fraction of deamidated protein after heating to various temperatures. A solution of 100 μM HPr in 10 mM NaP_i, pH 7.0, in a thin glass tube was heated at 1 °C/min in a waterbath. Fourteen 50 μL aliquots were taken at temperatures between 24 and 93 °C and immediately cooled on ice. The samples were loaded on a mono-Q column using the SMART system from Pharmacia and eluted with a gradient from 0 to 150 mM NaCl in 50 mM Tris, pH 8.3. HPr and the deamidated forms HPr-1 and HPr-2 eluted from the column at a 55, 80, and 112 mM NaCl, respectively, as observed from the absorption at 259 nm. The fractions of the different forms of HPr were calculated from the area under each peak, assuming that the molar extinction of all species is the same.

Equilibrium Unfolding and Refolding by Guanidine Hydrochloride (GdnHCl)

Circular Dichroism (CD). All CD studies were performed on either an Aviv 62A DS spectrometer in Groningen or a Jasco 720 spectrometer in Oxford using a quartz cuvet with a path length of 1 mm for all far-UV CD measurements and of 1 cm for near-UV CD measurements. The transition curve at 20 °C was obtained using the Job method, recording initially far-UV CD spectra of samples of 20 μM HPr solutions in 100 mM NaP_i, pH 7.0, containing 0 and 4.0 M GdnHCl. These samples were then mixed to produce samples with identical protein concentrations but containing different amounts of GdnHCl. After 20 min of equilibration, spectra were recorded of both samples and the procedure was repeated until mixing resulted in solutions of ca. 2.0 M GdnHCl. Far-UV CD spectra were recorded from 250 to 210 nm. Near-UV spectra were recorded from 290 to 250 nm at five different GdnHCl concentrations equally spaced over the transition curve. Five separate samples at different GdnHCl concentrations were diluted once to check whether the GdnHCl-induced unfolding of HPr is reversible. These solutions were equilibrated for at least 30 min before recording their spectra.

Denaturation was monitored by following the change in ellipticity (θ) at 222 nm in the far UV or by following the difference in ellipticity at 261 and 258 nm for the near UV transition. For analysis of the transition curve a modification of the method of Santoro and Bolen (*23*) was used, using the curve fitting methods in the Kaleidograph software (Synergy Software, PCS Inc.). A single GdnHCl denaturation curve described by observable y_{obs}, can be fitted to eq 1:

$$y_{obs} = (y_N + a_N[\mathrm{GdnHCl}])/(1 + \exp[[m[\mathrm{GdnHCl}] - \Delta G_{H_2O}]/RT]) + (y_U + a_U[\mathrm{GdnHCl}])\{\exp[[m[\mathrm{GdnHCl}] - \Delta G_{H_2O}]/RT]/(1 + \exp[[m[\mathrm{GdnHCl}] - \Delta G_{H_2O}]/RT])\} \quad (1)$$

with y_N, a_N, y_U, a_U, m, and ΔG_{H_2O} as fitting parameters. This equation combines the linear extrapolation method (LEM; *22*) with the two-state assumption for the unfolding reaction $N \overset{K_U}{\rightleftarrows} U$. ΔG_{H_2O} is the free energy in the absence of GdnHCl, m is the value which reflects the steepness of the unfolding transition, y_N, a_N and y_U, a_U are extrapolated from the pre- and post-transitional regions of the transition curve, and K_U is the equilibrium constant of unfolding.

8-Anilino-1-naphthalenesulfonic Acid (ANS) Fluorescence. Emission spectra from 400 to 600 nm were recorded on 5 μM HPr in 100 mM NaP_i, pH 7.0, the solutions containing 200 μM ANS in different concentrations of GdnHCl at 20 °C on a Perkin Elmer LS 50B fluorimeter, again using the Job method. Initial samples of HPr contained 0 and 4.0 M GdnHCl. The intensity at 472 nm was used to monitor the changes upon addition of GdnHCl. Data were fitted using eq 1.

Nuclear Magnetic Resonance (NMR). One-dimensional (1D) ^{1}H-NMR and two-dimensional (2D) ^{1}H−^{15}N heteronuclear single-quantum correlation (HSQC) spectra were recorded on samples containing 1.1 mM ^{15}N-enriched HPr in 100 mM NaP_i, pH 7.0, in different concentrations of GdnHCl at 20 °C on a Varian Unity Plus 500 spectrometer, again using the Job method. Initial samples of HPr contained 0 and 3.7 M GdnHCl (H_2O/D_2O: 93%/7%). To check the reversibility of the unfolding process an HSQC spectrum was recorded of a sample obtained after removal of the GdnHCl by washing the final 2.0 M GdnHCl sample with 100 mM NaP_i buffer, pH 7.0, using centricons. The 90° pulse length was adjusted to compensate for the increasing ionic strength

upon addition of GdnHCl. ^{1}H chemical shifts are relative to sodium 2.2-dimethyl-2-silapentane-5-sulfonate (DSS), and ^{15}N chemical shifts are expressed relative to liquid ammonia (*24*). Time-proportional phase incrementation (TPPI; *25*) was used to discriminate between positive and negative $\omega1$ (^{15}N) frequencies. Typically in the HSQC experiment: maximum t_1 and t_2 values were 128 ms and 154 ms, respectively, and spectral widths in the $\omega1$ (^{15}N) and $\omega2$ (^{1}H) domains were 2000 and 6666 Hz. The ^{1}H carrier was positioned on the water resonance, and during the acquisition period ^{15}N-decoupling was achieved by a broadband Waltz decoupling sequence. Water was suppressed using gradients. SNARF (Frans van Hoesel, Groningen) was used to process, visualize, and analyze the NMR data sets. The change in intensity of 56 out of 82 residue ^{1}H$-^{15}$N native cross peaks, and 13 out of 82 unfolded cross peaks could be followed upon addition of GdnHCl. The average intensity changes are used to describe the denaturation curve. Data were fitted using eq 1, and plotted as fraction folded or unfolded for direct comparison with results from CD.

Equilibrium Unfolding and Refolding by Temperature

Differential Scanning Calorimetry (DSC). All calorimetric measurements were performed on a MCS calorimeter from Microcal Inc. Most experiments were carried out at a scanning rate of 60 °C/h over a temperature range of 10−100 °C. No scan-rate dependency on the transition was observed from 12 °C/h up to 120 °C/h. Two consecutive scans were performed on each sample to check for reversibility. The DSC cells were operated under an N_2 pressure of 1.0−1.5 bar (*26*). HPr solutions of 50 μM were dialyzed overnight at 4 °C against buffer containing the required amount of GdnHCl. Dialyzed protein and dialysis buffer were used to load the sample and reference cells, respectively. Experimental data were corrected for small mismatches between the two cells by subtracting a buffer vs buffer base line prior to data analysis. After normalising to concentration a chemical base line calculated from the progress of the unfolding transition was subtracted and a two-state fit to the data was performed as implemented in the software package Origin (Microcal Software, Inc.). DSC scans presented in this work were performed on solutions containing approximately 50 μM HPr in 10 mM NaP_i, pH 7.0, in the absence of GdnHCl or 10 mM KP_i, pH 7.6, in the presence of 0, 0.5, 1.0, and 1.5 M GdnHCl. Salt effects were checked by running scans on HPr in 10 mM KP_i, pH 7.6, solutions containing 50, 100, 200, and 400 mM NaCl, respectively.

Circular Dichroism (CD). Temperature-induced unfolding was followed by monitoring the change in ellipticity at 222 nm of a 19 μM solution of HPr in 100 mM NaP_i, pH 7.0. Samples were heated using a scan rate of 45 °C/h. Data were fitted to eq 2:

$$y_{obs} = (y_N + a_N T)/(1 + \exp[[-\Delta H_m/T + \Delta H_m/T_m]/R]) + (y_U + a_U T)\{\exp[[-\Delta H_m/T + \Delta H_m/T_m]/R](1 + \exp[[-\Delta H_m/T + \Delta H_m/T_m]/R])\} \quad (2)$$

with y_N, a_N, y_U, a_U, ΔH_m, and T_m as fitting parameters. This equation is an extension of the van't Hoff equation, where ΔH_m and ΔS_m are the enthalpy and entropy changes at the transition temperature T_m, respectively. Since at T_m, $\Delta G = 0$, ΔS_m can be obtained from $\Delta H_m = T_m \Delta S_m$. The pre- and post-transitional regions of the transition curve are described by the terms $y_N + a_N T$ and $y_D + a_D T$, respectively.

Temperature-induced unfolding was also followed by monitoring the change in ellipticity at 222 nm of 18 μM solutions of HPr in 10 mM NaP_i, pH 7.0, containing increasing amounts of GdnHCl. These data can also be fitted to eq 2, but instead the exponential term includes a term for the change in heat capacity as described by the Gibbs−Helmholtz relationship (eq 3):

$$\Delta G(T) = \Delta H_m(1 - T/T_m) - \Delta C_p[(T_m - T) + T \ln(T/T_m)] \quad (3)$$

Kinetics of Unfolding and Refolding

Stopped-Flow CD. The stopped flow CD measurements at 222 or 225 nm (far-UV) were performed on either a Jasco 720 circular dichrograph equipped with a Biologic SFM3 stopped-flow module in Oxford or a Biologic stopped-flow CD equipped with double detection for both CD and fluorescence in Gif-sur-Yvette. HPr (2 mg/mL) in 6.0 M GdnHCl was rapidly mixed to give an 11-fold dilution in 100 mM NaP_i, pH 7.0, buffer to initiate refolding at 5, 9.5, 19.5, and 20 °C. Refolding at 19.5 °C was carried out in the absence and presence of 200 μM ANS to determine whether binding of ANS affects the refolding rate of HPr. Under these conditions, the ellipticity at 225 nm as well as the total fluorescence above 314 nm (excitation wavelength of 225 nm) were simultaneously detected. Refolding kinetics were fitted to either a single (CD) or double-exponential (ANS fluorescence) using the Kaleidograph software.

8-Anilino-1-Naphthalenesulfonic Acid (ANS) Fluorescence. For ANS fluorescence experiments an excitation wavelength of 350 nm was used, and total fluorescence above 390 nm was monitored using an Applied Photophysics SX.17MV stopped-flow spectrofluorimeter (APP). Typically, 1 mg/mL HPr solution unfolded in GdnHCl was diluted 11-fold with 100 μM ANS in 100 mM NaP_i, pH 7.0, buffer to initiate refolding. Refolding kinetics were fitted to a double exponential using the Kaleidograph software.

Real Time NMR Spectroscopy. NMR spectra were recorded using a home-built NMR spectrometer operating at 600.2 MHz and processed using FELIX (Hare Research). The spectral width was 8000 Hz. The water resonance was saturated by weak on-resonance irradiation during the 0.5 s relaxation delay. Chemical shifts are expressed relative to DSS. For all refolding experiments 50 μL of 100 mg/mL HPr in 6.0 M GdnHCl, pH 7.0, was diluted into a 500 μL volume of refolding buffer (100 mM NaP_i, pH 7.0). The final protein concentration in all NMR samples was 0.85 mM. Five hundred twelve 1D NMR spectra with two scans each were recorded for refolding at 2.8 °C with an acquisition time of 0.256 s. To initiate the refolding of HPr, denatured protein was injected through a Teflon transfer line into an NMR tube inserted inside the NMR probe, by means of a pneumatically driven syringe (7 bar pressure) at a fixed time point during the recording of the 512 1D FID's (*3*). The stability of the spectrometer was high enough for measurement to be made without locking on the deuterium signal

(*3*). Refolding kinetics were fitted to a single exponential using the Kaleidograph software.

GdnHCl and Temperature Dependence of the Folding Kinetics

GdnHCl Dependence. The dependency of the refolding and unfolding rates of HPr on the final GdnHCl concentration was determined by following the ANS fluorescence at 20 °C using the APP stopped-flow fluorimeter. HPr dissolved either in 0 or 6.45 M GdnHCl was diluted 11-fold into refolding buffers containing the required amount of GdnHCl in 100 μM ANS, 100 mM NaP_i, pH 7.0, to follow its unfolding and refolding, respectively. The refolding rate at the final concentration of GdnHCl of 0.36 M was obtained by diluting the initially unfolded HPr in 4.0 M GdnHCl into a solution of 100 μM ANS in 100 mM NaP_i, pH 7.0. The refolding/unfolding buffers were obtained by mixing two 100 μM ANS, 100 mM NaP_i, pH 7.0, stock solutions containing 0 M and 6.45 M GdnHCl, respectively. For a two-state transition, the refolding and unfolding kinetics can be described by eq 4:

$$\ln k_{obs} = \ln[k_f^{H_2O} \exp(-m_{k_f}[\text{GdnHCl}]) + k_u^{H_2O} \exp(m_{k_u}[\text{GdnHCl}])] \quad (4)$$

where the observed rate constant at a given GdnHCl concentration k_{obs} is described by the refolding and unfolding processes according to eqs 5 and 6, respectively:

$$\ln k_f = \ln k_f^{H_2O} - m_{k_f}[\text{GdnHCl}] \quad (5)$$

$$\ln k_u = \ln k_u^{H_2O} + m_{k_u}[\text{GdnHCl}] \quad (6)$$

where $k_f^{H_2O}$ and $k_u^{H_2O}$ are the rate constants of folding and unfolding in water, respectively, and m_{k_f} and m_{k_u} the slopes of the two linear halves of the curve. ΔG_{H_2O} can be calculated from the two-state assumption where the equilibrium constant for unfolding K_U is defined by $K_U = [U]/[N] = k_u/k_f$. Similarly, the m value can be calculated from the kinetic data using the relationship $m = m_{k_f} + m_{k_u}$. The concentration of GdnHCl at which 50% of the protein is denatured, c_M, can be calculated according to eq 7:

$$c_M = \frac{\ln(k_f^{H_2O}/k_u^{H_2O})}{(m_{k_f} + m_{k_u})} \quad (7)$$

Temperature Dependence. The dependency of the refolding rate of HPr from 6.0 M GdnHCl on temperature was measured by following ANS fluorescence at different temperatures ranging from 2.8 to 40 °C. Experimental details are as described above.

RESULTS

Equilibrium Unfolding and Refolding by GdnHCl and Temperature

Figure 1 shows CD spectra of HPr in its native state and following denaturation induced by GdnHCl and heat. No significant residual ellipticity is present in the far-UV region when the protein is denatured by GdnHCl, while substantial ellipticity remains after denaturation by heat. Similar differences have been observed for denatured states of other proteins (*20, 27*−*29*) and arise from the variation of the unfolded protein ellipticity with temperature and concentration of GdnHCl, as is evident from Figure 5B (see later; *30, 31*). The weak near-UV CD signal in the native state arises from the four phenylalanine residues present in HPr and also disappears upon adding high concentrations of GdnHCl.

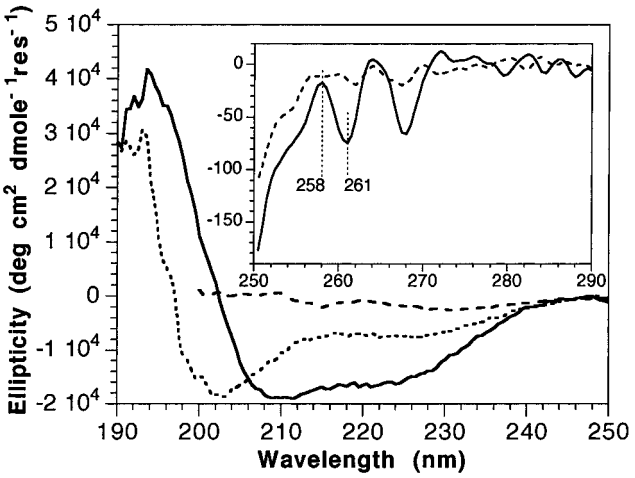

FIGURE 1: Far-UV and near-UV CD spectra of different states of HPr. Far-UV CD spectra of the native state (solid line), the heat-denatured state (dotted lines), and the GdnHCl-denatured state (dashed line) are shown. The inset shows the near-UV CD spectra of the native (solid line) and GdnHCl-induced denatured state (dashed line) of HPr.

GdnHCl-induced unfolding was also monitored by recording 1D ^1H and 2D $^1H-^{15}N$ HSQC NMR spectra. The top left panel of Figure 2A shows the characteristic highly dispersed HSQC spectrum of the native state (*21*). Above 3 M GdnHCl all native signals have disappeared and been replaced by signals characteristic of a denatured state (top right panel, Figure 2A). The latter spectrum still shows significant dispersion; 78 individual $^1H-^{15}N$ cross peaks can be identified. At 2 M GdnHCl, close to the midpoint of the transition (lower right panel, Figure 2A), the spectrum shows both native and denatured signals in a ratio of approximately 1:1. All spectra recorded at intermediate GdnHCl concentrations can be regarded as a linear combination of the native and the denatured spectra. No additional signals are observed at any concentration of GdnHCl, indicating the absence of any observable intermediate state upon unfolding of HPr. After removal of the residual GdnHCl by washing extensively with 100 mM NaP_i buffer, pH 7.0, the native state spectrum is fully recovered (lower left panel, Figure 2A), indicating that the unfolding process is reversible.

The intensity changes resulting from addition of GdnHCl for 56 out of the 82 observable backbone $^1H-^{15}N$ spin pairs of the native state could be followed. All cross peaks except two show the same dependency on GdnHCl as shown in Figure 2B. Their transition midpoints, c_M, are all close to the mean of 2.19 M. The two exceptions are Ala10 (A10) and active-site residue His15 (H15), whose cross peak intensities decrease at lower concentrations of GdnHCl than those of other residues (Figure 2C). Faster exchange of these protons with water or change in relaxation behavior in the presence of GdnHCl would result in an additional decrease in intensity. Whether this is indeed the case, or whether the

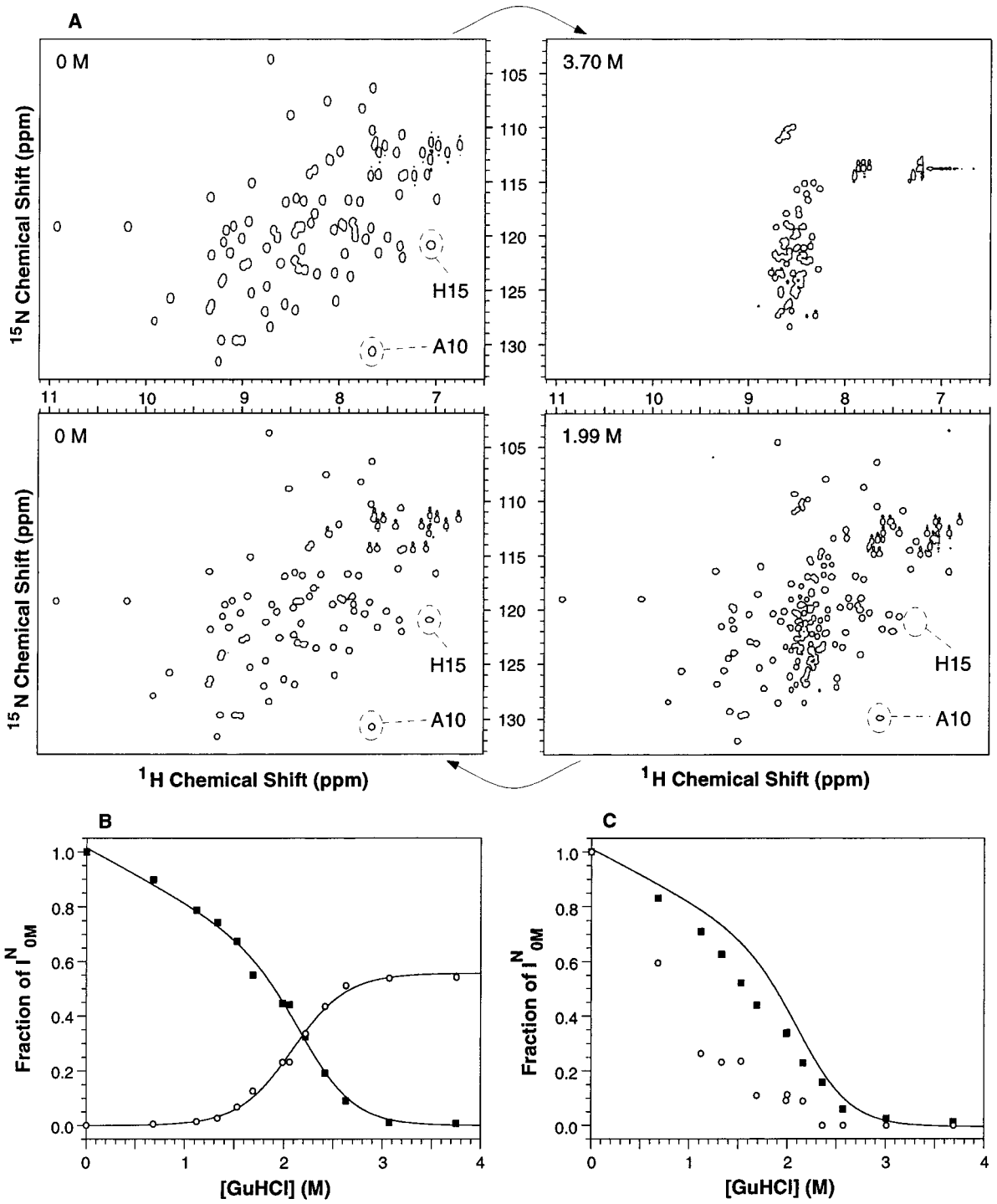

FIGURE 2: 2D ^{1}H−^{15}N HSQC NMR spectra of HPr and signal intensity changes at different stages during the denaturation by GdnHCl. (A) Spectra showing the transition from the native to the fully denatured state at 3.70 M GdnHCl (top), and spectra showing the transition of HPr close to the midpoint of the denaturation at 1.99 M GdnHCl and after washing this sample extensively (bottom). The latter spectrum is closely similar to the native state spectrum in accord with the reversibility of the unfolding. The transitions are indicated by arrows. At ~2.0 M GdnHCl all native signals are still observable, while that one of active-site residue His15 (H15) has disappeared. The corresponding ^{1}H−^{15}N cross peak is highlighted together with that of Ala10 (A10). (B) Change in average signal intensity of the native state (■) and the denatured state (○) plotted as the fraction of the native state intensity at 0 M (I^{N}_{0M}). Solid lines represent fits to eq 1, and the corresponding best fit parameters are given in Table 1. Note that the intensity of the fully denatured state is ~58% of that of the initial state at 0 M GdnHCl. (C) Changes in intensity of A10 (■) and H15 (○) upon addition of GdnHCl. Again intensities are scaled as a fraction of their native state intensity at 0 M for direct comparison with the average intensity change plotted by the solid line (best fit, Figure 2B).

greater decrease in intensity arises from a more site-specific effect by the interaction with GdnHCl, is not understood. In addition to following the disappearance of the native state signals, the appearance of 13 ^{1}H−^{15}N cross peaks of the denatured state could be followed upon addition of GdnHCl. Their mean intensity at 3.70 M GdnHCl is only 58% of that of the native state at 0 M GdnHCl (Figure 2B) due to the change in the quality factor of the probe (*Q* factor) on adding high amounts of salt (*32*). Similar effects have been observed in unfolding studies of lysozyme (*33*).

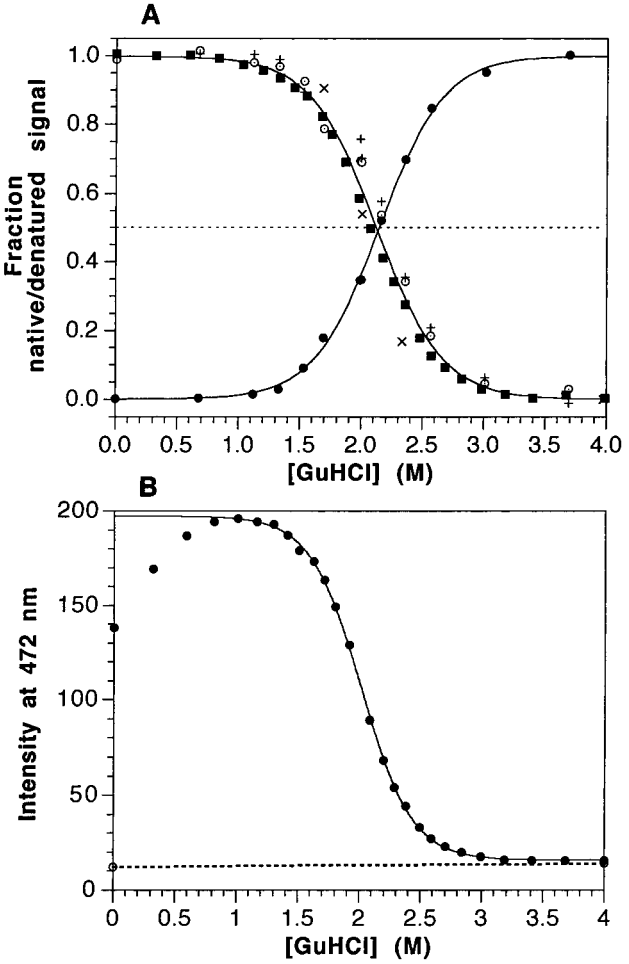

FIGURE 3: GdnHCl denaturation curves for HPr monitored by CD, NMR, and ANS fluorescence at 20 °C. (A) Changes are plotted as the fraction of native signal for all transition curves [except where the fraction of the denatured signal is plotted in the case of the appearance of denatured state $^1H-^{15}N$ cross peaks by NMR (●)]. Ellipticity at 222 nm (far-UV; ■); difference in ellipticity at 261 and 258 nm (near-UV, ×); average native backbone $^1H-^{15}N$ NMR cross peaks (○); native signal of the C^dH_3 of Leu77 (+). Solid lines represent the fit to eq 1, and the corresponding best fit parameters are given in Table 1. (B) Denaturation followed by ANS fluorescence. The fluorescence enhancement increases initially upon adding small amounts of GdnHCl but then gradually decreases as the denaturation takes place. The dotted line represents the fluorescence intensity of ANS in the absence of protein. The solid line represent the fit to eq 1 excluding the first 4 points, and the corresponding best fit parameters are given in Table 1.

Figure 3 shows the denaturation curves of HPr at 20 °C monitored by different techniques; the thermodynamic parameters obtained from fitting the raw data to eq 1 are summarized in Table 1. For comparison the CD and NMR data are all plotted as the fraction of the unfolded or the folded signal present under given conditions. The near-UV and far-UV denaturation curves coincide, as do the curves monitoring the disappearance of native backbone and side-chain NMR signals and the appearance of the unfolded signals. CD spectra of five HPr samples containing different amounts of GdnHCl were recorded after 1:1 dilution into refolding buffer to check for reversibility. All samples showed values for the ellipticity at 222 nm similar to those expected from the denaturation curve, confirming the complete reversibility of the unfolding process in agreement with the full recovery of the native state NMR spectrum after unfolding.

Denaturation monitored by ANS fluorescence shows some interesting characteristics (Figure 3B). Initially the fluorescence enhancement increases upon adding GdnHCl until it reaches a maximum at about 1.2 M GdnHCl. At higher concentrations, the intensity decreases as a result of the unfolding of the protein. We excluded this first part of the curve in fitting the data to eq 1 (solid line Figure 3B); the thermodynamic parameters derived from the fit are given in Table 1. Thus, we neglect the effect of the increase in ANS binding at low concentrations of GdnHCl; as a result the thermodynamic parameters are slightly higher than those obtained using CD and NMR spectroscopy techniques. The ΔG for unfolding calculated from the latter two experiments are better estimates; the thermodynamic parameters obtained from the ANS binding experiment should be compared with the value obtained from kinetic folding experiments using ANS as probe (see later). The increase in ANS fluorescence observed here might be correlated to the greater decrease in intensity of the Ala10 and His15 cross peaks in the unfolding experiments monitored by NMR described above.

Figure 4 presents DSC profiles for HPr under different conditions during thermal denaturation. The unfolding was found to be independent of the scan rate. This shows that the native and unfolded forms of HPr equilibrate rapidly in comparison with the time constant of the calorimeter (*26*) and that equilibrium thermodynamics apply. Nicholson and Scholtz (*20*) found that transitions monitored by far UV CD were more than 95% reversible after heating *E. coli* HPr solutions in the absence and presence of urea to 90 °C, and that some reversibility was lost due to products of urea decomposition. We find that thermal unfolding of HPr, even in the absence of denaturant, is not completely reversible; there are shifts in transition temperature and a lowering of the enthalpy of unfolding when samples of HPr were rescanned after thermal denaturation up to 90 °C, as shown in Figure 4A. Such a transition curve can no longer be described using a two-state model of unfolding. The observed irreversibility is most likely due to deamidation of the two asparagine residues in the unfolded state of HPr resulting in two modified forms of the protein, HPr-1 and HPr-2 (*34*). From these studies it is known that the rate of deamidation is substantially greater at high temperatures and at high pH. To confirm this, a rescan was recorded after thermal denaturation up to only 70 °C. The inset in Figure 4A shows that this transition profile is closely similar to that observed for the first scan.

To explore this issue further, populations of HPr, HPr-1 and HPr-2 were monitored as a function of temperature by HPLC. At 70 °C, well above the T_m, more than 90% of HPr is in its non-deamidated form. So from both DSC and HPLC we can conclude that unfolding precedes the deamidation process, and, therefore, that a two-state assumption may be applied to interpret the thermal denaturation data. Figure 4B shows DSC denaturation profiles of HPr dissolved in different amounts of GdnHCl. Thermodynamic parameters derived from these DSC measurements are summarized in Table 1. Van't Hoff enthalpies correspond well with the calorimetric enthalpies indicating that the heat induced unfolding of HPr is indeed a two-state process.

Table 1: Analysis of GdnHCl and Heat Denaturation Monitored by DSC, CD, NMR, and ANS Fluorescence at Equilibrium and by ANS Fluorescence from Kinetic Studies

	ΔH (kJ mol^{-1})	T_m (°C)	ΔG (kJ mol^{-1})	m (kJ mol^{-1} M^{-1})	c_M (M)
		DSC			
10 mM P_i, pH 7.0	268.4[a]/284.3[b]	64.3			
10 mM P_i, pH 7.6					
0 M GdnHCl	306.0/325.2	60.5			
0.5 M GdnHCl	244.1/255.8	55.0			
1.0 M GdnHCl	219.0/224.0	49.0			
1.5 M GdnHCl	170.1/167.6	40.4			
		CD			
10 mM P_i, pH 7.0	287.9 ± 4.5	65.5 ± 0.1			
100 mM P_i, pH 7.0	322.9 ± 2.8	64.6 ± 0.1	19.1 ± 0.5	9.1 ± 0.3	2.09 ± 0.09
		NMR[c]			
100 mM P_i, pH 7.0					
native			19.8 ± 1.7	9.0 ± 0.8	2.19 ± 0.27
unfolded			20.0 ± 0.8	9.3 ± 0.4	2.14 ± 0.13
		ANS Fluorescence			
100 mM P_i, pH 7.0					
equilibrium[d]			23.3 ± 0.8	11.6 ± 0.4	2.01 ± 0.10
kinetics[e]			21.6 ± 0.4	10.8 ± 0.24	2.01 ± 0.06

[a] Calorimetric ΔH. [b] Van't Hoff ΔH. [c] Mean values for the 56 native state and 13 denatured state amide $^1H-^{15}N$ cross peaks. [d] Values obtained from Figure 3B neglecting the increase in ANS fluorescence at low concentrations of GdnHCl, see text. [e] Values obtained using eqs 4−7 (Figure 10C).

Figure 5A shows the denaturation curve of HPr in 100 mM NaP_i buffers at pH 7.0 monitored by the change in ellipticity at 222 nm. The enthalpy for unfolding is higher than the van't Hoff enthalpy found for HPr in lower phosphate concentrations by DSC (10 mM, Figure 4A), while the transition temperatures obtained from these experiments are closely similar (Table 1). Unfolding of HPr in 10 mM NaP_i at pH 7.0 followed by CD (Figure 5B) results in similar thermodynamic parameters to those determined by DSC. DSC experiments carried out at higher pH also result in higher enthalpies of unfolding but lower transition temperatures (Figure 4B and Table 1). High concentrations of phosphate and increasing pH, therefore, both result in an increase in ΔH but have different effects on the transition temperatures. Figure 5B shows thermal unfolding curves of HPr at different GdnHCl concentrations. At concentrations above 1 M cold denaturation can be observed. The denatured state base line, which corresponds to the transition curve at high concentrations of GdnHCl, can be adequately described by a second order polynomial. The line coincides with the ellipticities for the GdnHCl denatured state at low temperatures and the heat-denatured state in the absence of GdnHCl as shown in Figure 1, indicating that both denatured states represent the same thermodynamic state as shown for other proteins (*30*, *31*).

Kinetics of Refolding

Figure 6 shows the time course after initiation of refolding of HPr from 6.0 M GdnHCl at 19.5 °C as simultaneously monitored by far-UV CD and ANS fluorescence. No events in the dead-time of the stopped-flow experiment were observed either by CD or by ANS fluorescence. The refolding kinetics followed by CD fit a single exponential rate law at all temperatures studied (5, 9.5, 19.5, and 20 °C). In addition, stopped-flow experiments monitoring the intrinsic fluorescence of a single tryptophan mutant of HPr shows single exponential refolding kinetics (unpublished results). In contrast, two kinetic phases can be observed when refolding is monitored by ANS fluorescence. No changes in the kinetics of these phases were observed when the concentration of HPr was reduced from 1 to 0.5 mg/mL prior to initiation of the folding reaction. The best fit parameters to a single (CD) and a double-exponential (ANS fluorescence) rate law are collected in Table 2. The time constant for the faster phase is closely similar to that of far-UV CD techniques, 0.46 and 0.50 s, respectively, and is not affected by the presence of ANS (insert Figure 6B). The time constant for the slower phase observed by ANS fluorescence is 10.8 s. Such slow stages in folding have often been attributed to proline *cis*−*trans* isomerization (*35*). The overshoot in ANS fluorescence indicates the existence of an intermediate state that preferentially binds ANS. The native state itself also binds ANS, most probably to the hydrophobic patch present in the binding interface with domain A of enzyme II (*36*, 37).

Figure 7 shows a series of 1D NMR spectra recorded during the refolding of HPr at 2.8 °C following rapid injection of the protein denatured in 6.0 M GdnHCl into a refolding buffer at pH 7.0. The spectra were recorded at 1.51 s intervals, the first scan being completed 0.75 s after injection. In earlier work (*3*) we found that mixing is complete within a few seconds; the evolution of the NMR spectrum shown in Figure 7 may therefore be attributed solely to the structural changes occurring during refolding. Figure 8 shows the first (Figure 8B) and the last (Figure 8C) spectra of the experiment illustrated in Figure 7, compared with the spectrum of HPr in 6.0 M GdnHCl (Figure 8A), where the protein is highly unfolded. Comparison of the spectra after long refolding times (Figure 8C) with that of the native state shows they are identical, indicating that the native state has been fully regenerated in the refolding experiment. The spectra at the shorter refolding times (see Figure 7 and Figure 8B) are similar to that of the unfolded one depicted in Figure 8A with respect to chemical

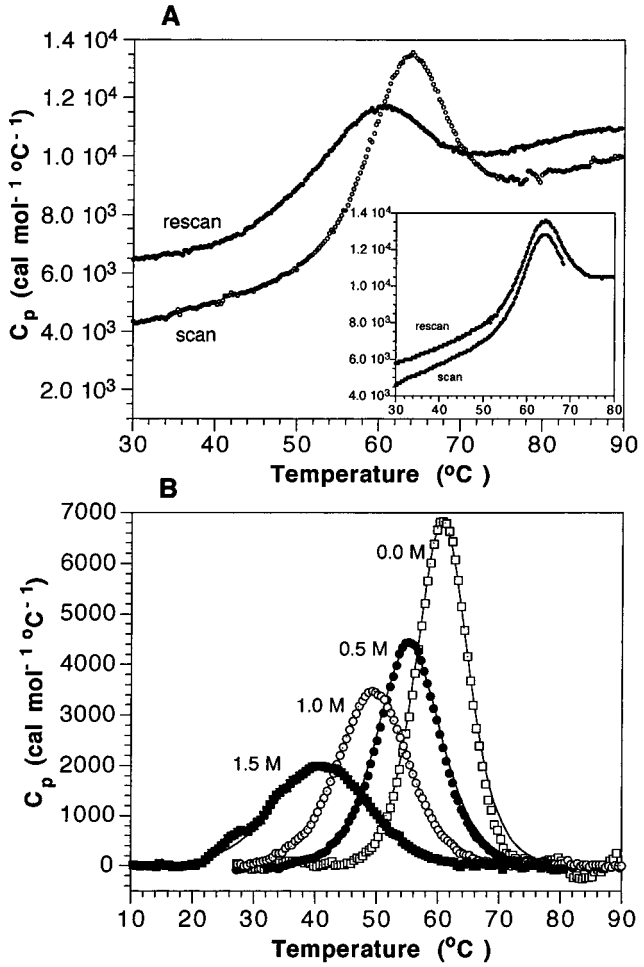

FIGURE 4: DSC scans of HPr under different conditions. (A) Scan and rescans of HPr in 10 mM NaP_i, pH 7.0, showing the incomplete reversibility upon heat denaturation when heated to 90 °C, but almost complete reversibility when heated to 70 °C (inset; for clarity, the rescan is displaced upward by 1000 cal mol^{-1} °C^{-1}). Thermodynamic parameters are summarized in Table 1. (B) DSC scans of HPr at different concentrations of GdnHCl in 10 mM KP_i, pH 7.6, buffer. GdnHCl concentrations were 0 M (□), 0.5 M (●), 1.0 M (○), and 1.5 M (■). Data are plotted as described in the text. Solid lines represent best fits to a two-state model of unfolding as implemented in the software package Origin. Thermodynamic parameters are summarized in Table 1. The values for T_m and the corresponding ΔH_m values were used to determine ΔC_p shown in Figure 12.

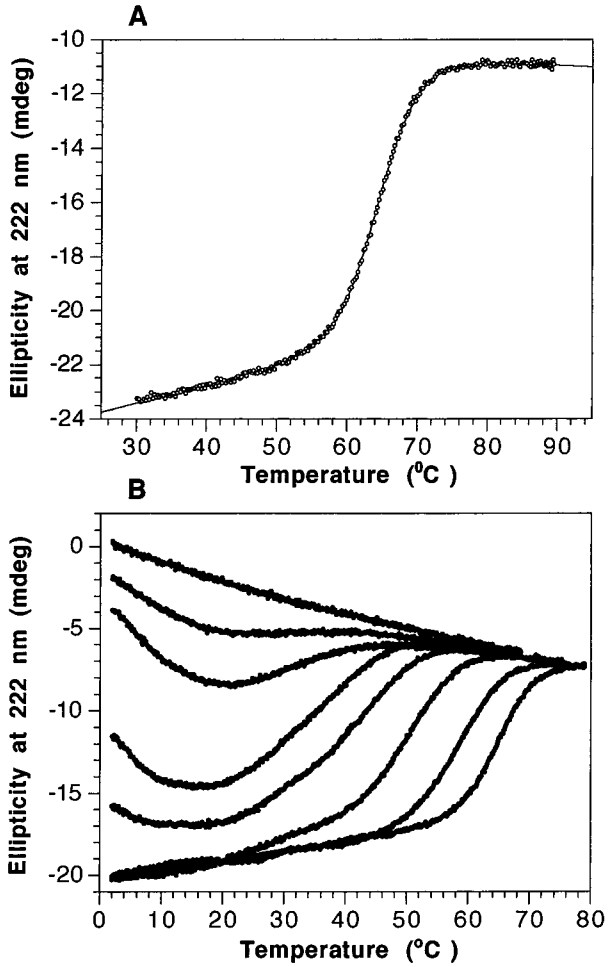

FIGURE 5: Thermal unfolding curves for HPr at pH 7.0. (A) Denaturation followed by the change in ellipticity at 222 nm (far-UV CD) for HPr in 100 mM NaP_i, pH 7.0. The curve through the data represents the fit to eq 2, and the corresponding best fit parameters are given in Table 1. (B) Denaturation followed by the change in ellipticity at 222 nm for HPr in 10 mM NaP_i, pH 7.0, at different GdnHCl concentrations (0, 0.34, 0.75, 1.17, 1.39, 1.78, 1.98, and 2.80 M). These curves were fitted to eq 2 in which the exponential term is replaced by a ΔC_p dependent term as described by eq 3. The values for T_m and the corresponding ΔH_m values were used to determine ΔC_p shown in Figure 12. The variation of the unfolded protein (2.8 M GdnHCl) ellipticity with temperature explains the difference in residual ellipticity in the far-UV spectra of the two denatured states shown in Figure 1.

dispersion. Lines are broader, reflecting residual inhomogeneity of the mixture at these early times. At times larger than ~5 s following the initiation of refolding, a series of peaks is visible in the NMR spectrum, corresponding to those of the native state. Analysis of the intensities of well-resolved and assigned peaks in the native spectrum from different regions of the protein (Figure 8D), including those of the upfield-shifted resonances of the side chain of Leu77 positioned in the hydrophobic core of HPr (*8*, *9*), show that they all develop at rates closely similar to each other and to the rate of the overall appearance of the native spectrum. The kinetics show single-exponential behavior and coincide, within experimental error, with the kinetics of the disappearance of signals assigned to the spectrum of the initial state, and to the faster phase monitored by ANS fluorescence. The best fit parameters to a single-exponential (NMR) and a double-exponential (ANS fluorescence) are given in Table 2. The kinetic data were used to reconstruct all spectra at intermediate time points between the first and the final spectrum by a linear combination of the latter two spectra; this is shown for two kinetic spectra at different refolding time points in Figure 9. The reconstructed spectra are closely similar to the experimental spectra; this indicates that all spectral changes observed during refolding can be solely attributed to a single, highly cooperative two-state transition from the denatured state into the native state.

GdnHCl and Temperature Dependence of the Folding and Unfolding Kinetics

Figure 10 shows the refolding (Figure 10A) and unfolding (Figure 10B) kinetics as a function of the final GdnHCl concentration as monitored by ANS fluorescence. The unfolding kinetics show monophasic behavior while the refolding kinetics at low GdnHCl concentrations can be

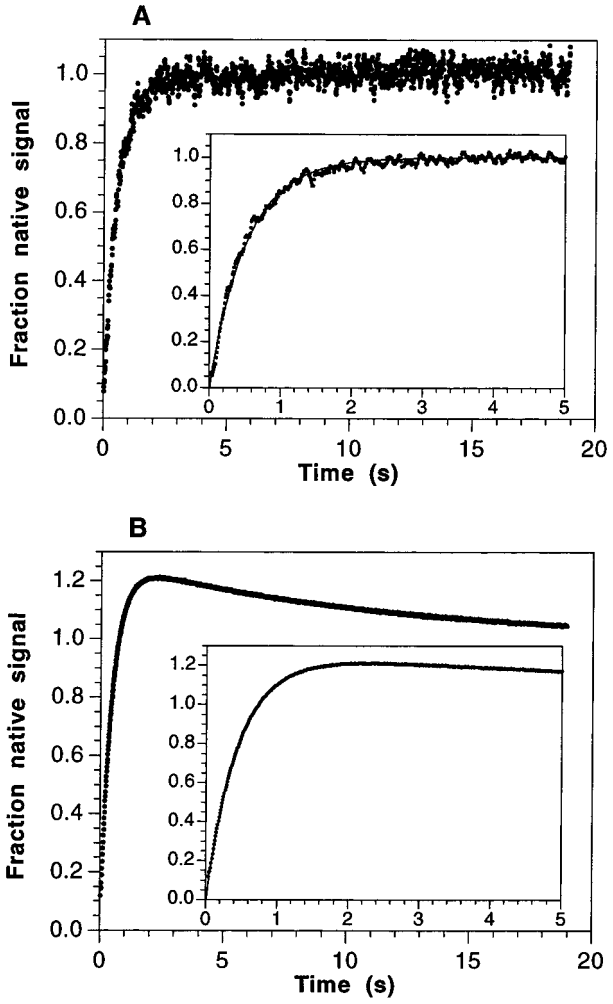

FIGURE 6: Refolding kinetics of HPr from 6.0 M GdnHCl. Measurements were at 19.5 °C and monitored by the change in ellipticity at 225 nm (A) in the presence of ANS and simultaneously recorded change in fluorescence enhancement upon ANS binding (B). Data are plotted as a fraction of the final native signal. The inset in A shows the refolding of HPr as monitored by CD in the absence of ANS. The inset in B shows the first 5 s of the refolding process as monitored by ANS fluorescence. Solid lines represent best fits to a single- or double-exponential term, and the corresponding best fit parameters are given in Table 2.

Table 2: Time Constants (τ) and Relative Amplitudes (A) of Refolding from 6.0 M GdnHCl for HPr at Different Temperatures (T) Obtained from CD, ANS Fluorescence, and NMR Experiments

technique	T (°C)	A_1 (%)	τ_1 (s)	A_2 (%)	τ_2 (s)
ANS	2.8	91.2	8.38	8.8	120.5
NMR[a]					
N	2.8	100	9.0		
U		100	7.6		
ANS	19.5	82.4	0.46	17.6	10. 8
CD[b]	19.5	100	0.51		
CD[c]	19.5	100	0.50		

[a] Kinetics of the appearance of the native state (N) Leu77 $C^{\delta}H_3$ resonance and the disappearance of the unfolded state (U) signal at 1.38 ppm indicated in Figure 8. [b] Far-UV CD measured in the absence of ANS (inset Figure 6A). [c] Far-UV CD measured in the presence of 200 μM ANS (Figure 6A).

described by double-exponential kinetics. The rate constant of the faster refolding phase decreases exponentially with GdnHCl concentration over the range 0−2.0 M (Figure 10C). The kinetics of the slower phase are more or less independent

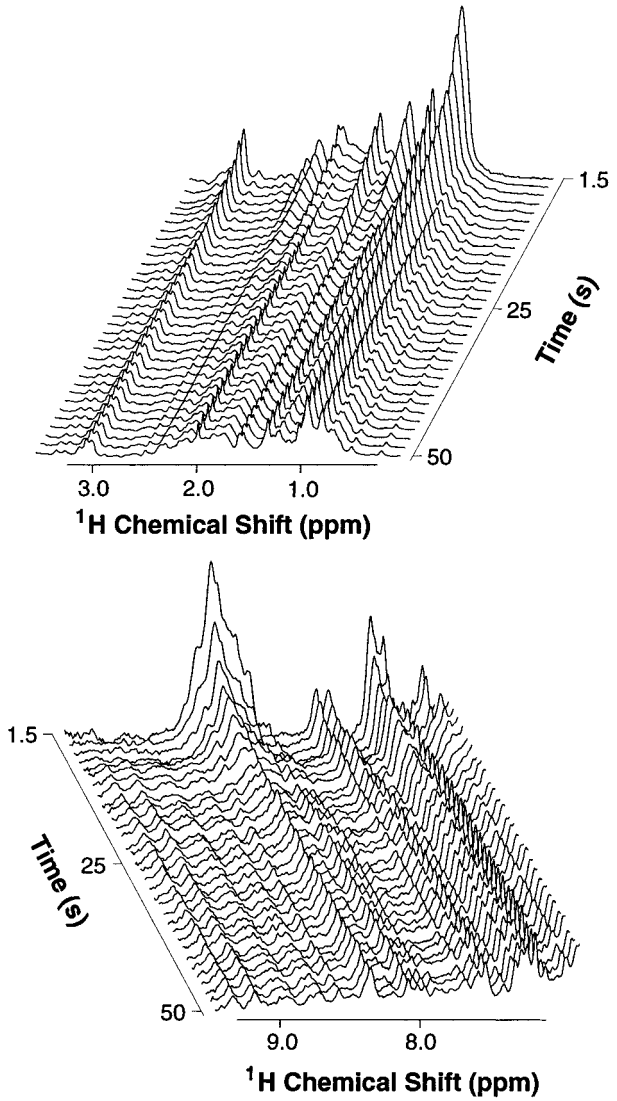

FIGURE 7: Stacked plot of 600 MHz 1D NMR spectra of HPr in H_2O at 2.8 °C. Spectra were recorded at incremented time points between 1.51 and 384 s after initiation of refolding from 6.0 M GdnHCl in 100 mM NaP_i, pH 7.0. The region shown at the top contains resonances from methyl and methylene groups, and that at the bottom from aromatic groups and amide protons.

of the final GdnHCl concentration at concentrations below 1 M but show strong dependency above 1 M. The relative amplitudes of both phases are strongly dependent on the final GdnHCl concentration; the slower phase diminishes significantly at high concentrations. The complete kinetics of folding and unfolding can be fitted to eq 4 which is based on a two-state transition. The calculated fits of the folding and unfolding data to eqs 5 and 6, respectively, are shown by solid lines in Figure 10C. The values for $k_f^{H_2O}$, $k_u^{H_2O}$, m_{k_f}, and m_{k_u} are 14.9 s^{-1}, 20.9 × 10^{-4} s^{-1}, 2.84 M^{-1}, and 1.58 M^{-1}, respectively. From these results, the equilibrium values for ΔG_{H_2O} and m were calculated as described in the Methods section and c_M from eq 7; they are listed in Table 1. The values for ΔG_{H_2O} and m calculated in this way are 21.6 kJ mol^{-1} and 10.8 kJ mol^{-1} M^{-1} and are slightly higher than those obtained from equilibrium experiments using CD and NMR but are similar to the values obtained by ANS fluorescence at equilibrium. We have shown (Figure 3B) that increasing concentrations of GdnHCl lead to an increase in fluorescence enhancement in equilibrium unfolding ex-

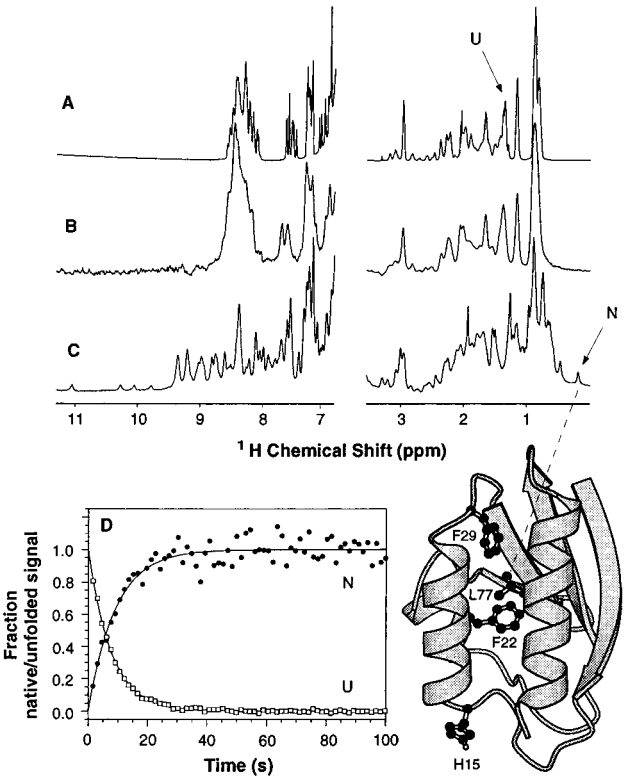

FIGURE 8: Refolding of HPr from 6.0 M GdnHCl in H_2O at 2.8 °C monitored by NMR (A) 600 MHz 1D ^{1}H NMR spectrum of HPr in 6.0 M GdnHCl in 100 mM NaP_i, pH 7.0. (B) Spectrum recorded 1.51 s (average over 2 scans) after initiating refolding from 6.0 M GdnHCl, in 100 mM NaP_i buffer, pH 7.0. (C) Average over the final 32 spectra (~6 min after injection) following complete refolding from 6.0 M GdnHCl, in 100 mM NaP_i buffer, pH 7.0. (D) Refolding kinetics of HPr from 6.0 M GdnHCl obtained from the real-time NMR measurement showing the disappearance of the unfolded signals at 1.38 ppm (U, □) and the appearance of the native signal of Leu77 $C^{\delta}H_3$ side chain (N, ●) indicated in spectrum A and C, respectively. The Molscript representation (*65*) shows the position of this methyl group in the hydrophobic core of HPr in close proximity to Phe22 and Phe29. In addition, the active site residue His15 is indicated. The solid lines represent the best fit to a single exponential and are given in Table 2.

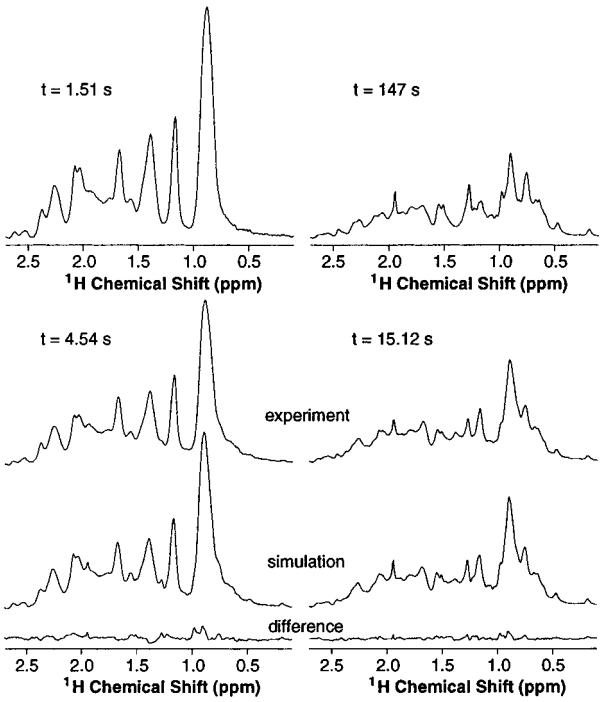

FIGURE 9: Reconstruction of NMR spectra at 4.54 s and 15.12 s during the refolding of HPr from 6.0 M GdnHCl in H_2O at 2.8 °C. The spectra were reconstructed by a linear combination of the first (top, $t = 1.51$ s) and last (top, $t = 147$ s) spectrum recorded after initiating refolding using a rate constant of 0.12 s^{-1} which is the average rate constant extracted from the analysis shown in Figure 8D. Only the upfield spectral regions are shown and are plotted in absolute intensity.

periments, indicating the presence of a state that either binds ANS stronger than the native state is or has relatively more hydrophobic surface exposed to the solvent upon adding GdnHCl. This could also explain the change in amplitude observed during the refolding kinetics shown in Figure 10A.

The refolding kinetics of HPr from 6.0 M GdnHCl at different temperatures were monitored by ANS fluorescence, far-UV CD, and NMR. While the relative amplitudes of the fast and slow phases in ANS fluorescence are strongly dependent on the final GdnHCl concentration, the dependency on the temperature is less pronounced. Upon increasing temperature the amplitude of the slower phase also increases. Figure 11A shows refolding of HPr monitored by ANS fluorescence at different temperatures; the fluorescence enhancement upon binding to the final native state after refolding completely decreases rapidly with temperature. The fluorescence, extrapolated from the intensity decrease with temperature, is expected to reach zero at ~52 °C; this temperature coincides with the temperature at the start of the heat induced unfolding transition (see Figures 4 and 5). Eyring plots [$\ln(k_f/T)$ versus $1/T$], for both the slow and fast phases are plotted in Figure 11B. The Eyring plot for the slower phase is linear over the temperature range investigated (2.8−40 °C). The activation parameters for folding can be calculated from the Eyring plot by using eq 8:

$$\ln(k_f/T) = \ln(k_B/h) + \Delta S_f^{\ddagger}/R - \Delta H_f^{\ddagger}/RT \qquad (8)$$

where k_f is the rate of folding, $\Delta S_f^{\ddagger}$ is the activation entropy of folding, $\Delta H_f^{\ddagger}$ is the activation enthalpy of folding, and h and k_B are Planck's and Boltzmann's constants, respectively. There is significant curvature in the Eyring plot for the temperature dependence of the faster refolding phase as can be seen in Figure 11B. Jackson and Fersht (*38*) also observed significant curvature in the Eyring plot of the fast refolding phase of chymotrypsin inhibitor 2 (CI2). Curvature in Eyring plots can be observed when there is a significant change in heat capacity between the initial state (denatured state in this case) and the transition state. Following the analysis described by Jackson and Fersht (*38*), the data can be fitted to eq 9:

$$\ln(k_f/T) = A + B(T_o/T) + C\ln(T_o/T) \qquad (9)$$

where

$$A = [-\Delta C_{pf}^{\ddagger} + \Delta S_f^{\ddagger}(T_o)]/R - \ln(h/k_B)$$

$$B = [\Delta C_{pf}^{\ddagger} - \Delta S_f^{\ddagger}(T_o)]/R - \Delta G_f^{\ddagger}(T_o)/RT_o$$

$$C = -\Delta C_{pf}^{\ddagger}/R$$

where $\Delta C_{pf}^{\ddagger}$ is the heat capacity change between the dena-

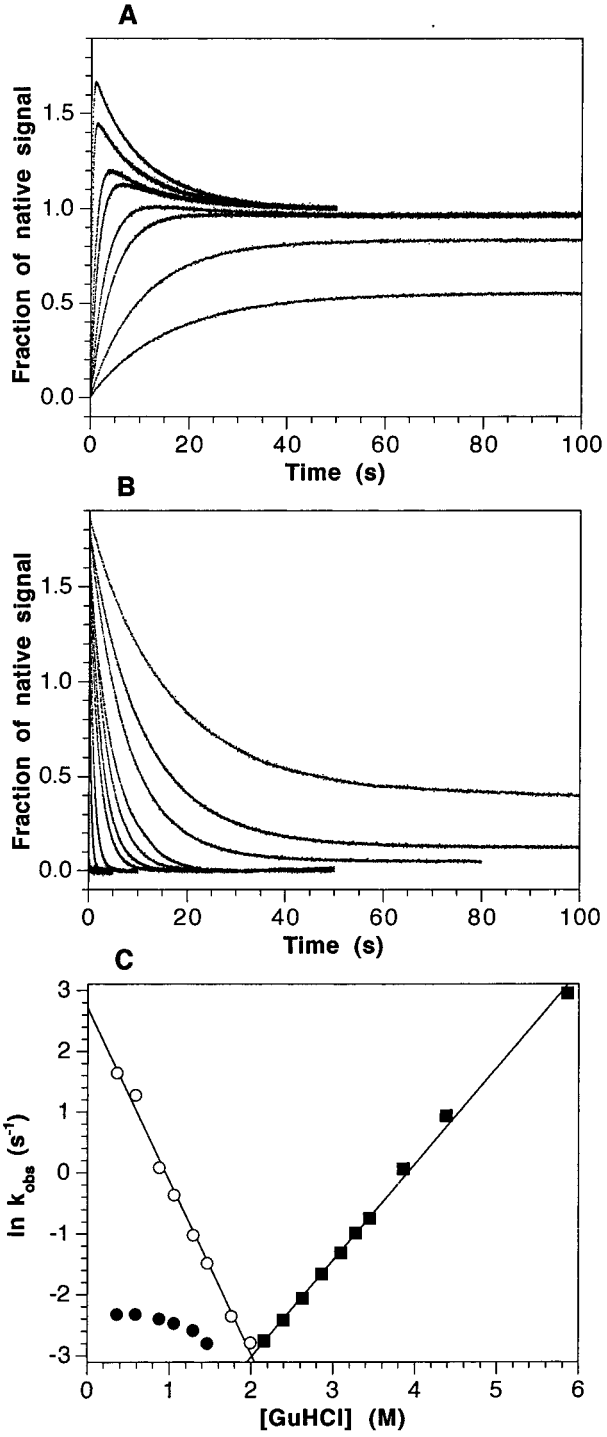

FIGURE 10: Refolding and unfolding kinetics at 20 °C at different GdnHCl concentrations monitored by ANS fluorescence. (A) Refolding kinetics fitted to a double exponential function. (B) Unfolding kinetics fitted to a single exponential function. (C) Logarithms of the rate constants of refolding for the fast phase (○) and slow phase (●), and for unfolding (■). Solid lines represent best fits to eqs 5 and 6 for the refolding and unfolding, respectively. Best fit parameters are given in the text. Values for ΔG_{H_2O} and m obtained from these kinetic data are given in Table 1 for comparison with the values obtained from equilibrium experiments.

tured state and the transition state, $\Delta S_f^{\ddagger}$ as described above, and $\Delta G_f^{\ddagger}$ is the activation energy of folding. The activation parameters for refolding of HPr at T_o = 20 °C were calculated from the fit of the data to eq 9. These results,

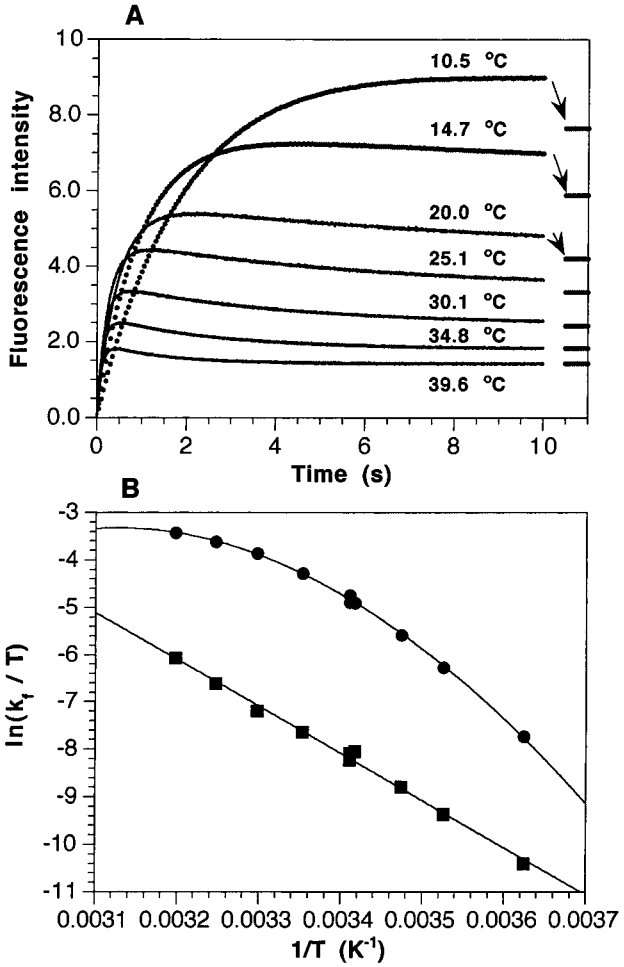

FIGURE 11: Refolding of HPr from 6.0 M GdnHCl at different temperatures monitored by ANS fluorescence. (A) Progression of folding at indicated temperatures. The final fluorescence intensity is indicated by a short line. Note the rapid decrease in fluorescence enhancement due to the loss of ANS binding to the native state. (B) Eyring plots of the faster refolding phase (●) and the slower refolding phase (■). Solid lines represent fits to eqs 8 and 9, respectively. Activation parameters derived from these fits are given in Table 3.

Table 3: Activation Parameters for the Fast and Slow Refolding Phases of HPr from 6.0 M GdnHCl into 100 mM NaP_i, pH 7.0

phase	$\Delta C_p^{\ddagger}$ (kJ mol^{-1} K^{-1})	$\Delta H^{\ddagger}$ (kJ mol^{-1})	$\Delta S^{\ddagger}$ (J mol^{-1} K^{-1})	$\Delta G^{\ddagger}$ (20 °C) (kJ mol^{-1})
slow[a]		82.3 ± 2.1	16.7 ± 7.5	
fast[b]	−3.22 ± 0.17	86.1 ± 0.4	56.0 ± 3.3	69.7 ± 0.1
				69.0 ± 0.1[c]

[a] Calculated from the Eyring plot for the slower phase (Figure 11B) using eq 8. [b] Calculated from the Eyring plot for the faster phase (Figure 11B) using eq 9. [c] Calculated from GdnHCl-dependent refolding for the faster phase (Figure 10C) under the same conditions: 0.55 M GdnHCl, 100 mM NaP_i, pH 7.0, 20 °C.

together from the results for the slow phase derived from eq 8, are summarized in Table 3.

DISCUSSION

In the previous section we have shown that the denaturation of HPr can be described as a two-state reaction from the following evidence: (i) all unfolding data can be fitted to a single transition curve using eqs 1−3, (ii) the transition is independent of the probe used to determine the state of

Table 4: Thermodynamic Parameters for the Folding of HPr

parameter	*E. coli* HPr[a]	*E. coli* HPr[b]	*B. subtilis* HPr[c]
ΔH_m (kJ mol^{-1})	284.3/287.9/322.9/325.2	316.8	242.9
T_m (°C)	64.3/65.5/64.6/60.5	63.5	73.4
T_m' (°C)[d]	−18.4/−18.1/−28.2/−30.9	−28.5	−18.0
ΔG_s (kJ mol^{-1})[d]	18.2/18.6/23.3/23.4	22.8	16.7
T_s (°C)[d]	22.0/22.7/16.1/13.6	16.3	26.0
ΔC_p (kJ mol^{-1} K^{-1})[e]	nd/6.3/nd/6.4	6.23	4.89
ΔC_p (kJ mol^{-1} K^{-1})[f]	5.18	5.18	5.43
ΔC_p (kJ mol^{-1} K^{-1})[g]	6.48	6.48	7.77
m (kJ mol^{-1} M^{-1})[h]	9.57 (GdnHCl)	4.85 (urea)	4.39 (urea)
m (kJ mol^{-1} M^{-1})[i]	10.53 (GdnHCl)	4.67 (urea)	4.81 (urea)
m (kJ mol^{-1} M^{-1})[j]	4.36 (urea)	10.69 (GdnHCl)	9.66 (GdnHCl)
c_M (M)[h]	2.11 (GdnHCl)	4.70 (urea)	3.88 (urea)
ΔASA (Å^2)[k]	6809 (4680/2129)	6809 (4680/2129)	7090 (5212/1878)

[a] Experimental values reported here for HPr in 10 mM phosphate at pH 7.0 using DSC, in 10 mM phosphate at pH 7.0 using CD, in 100 mM phosphate at pH 7.0 using CD, and in 10 mM phosphate at pH 7.6 using DSC, respectively. [b] Values from Nicholson and Scholtz (*20*). [c] Values for *B. subtilis* HPr obtained from Scholtz (*19*). [d] Parameters derived from the Gibbs−Helmholtz equation (eq 3; Figure 13). [e] ΔC_p calculated from a ΔH_m versus T_m analysis (Figure 12). nd, not determined. [f] ΔC_p calculated from the equation $\Delta C_p = -119 + 0.20\Delta$ASA (*39*). [g] ΔC_p calculated from the equation $\Delta C_p = 0.45\Delta ASA_{np} - 0.26\Delta ASA_p$ (*40*). [h] Experimental value for given denaturant. The *E. coli* HPr values are averaged over values given in Table 1. [i] m calculated from the equations: $m = 953 + 0.23$ASA and $m = 368 + 0.11$ASA for GdnHCl and urea, respectively (*39*). [j] m calculated from the equation $m_{GdnHCl} = -110 + 2.3M_{urea}$ using experimental values given above (*39*). [k] Values given are averaged over the *E. coli* NMR and X-ray structures (PDB entries 1HDN and 1POH, respectively). A model of unfolded HPr was generated using InsightII (Biosym) by giving the polypeptide chain extended dihedral angles. The accessible surface areas (ASA) of both the native and the extended chain were calculated using the program ACCESS (*63*), with a probe radius of 1.4 Å, a slice width of 0.25 Å, and atomic radii given by Richards (*64*). Values given are differences between the unfolded and native states of the protein. The nonpolar (ASA_{np}) and polar (ASA_p) ΔASA's are given in brackets, respectively. Values for *B. subtilis* HPr were obtained from Myers et al. (*39*).

the protein, in this work near and far UV CD, ANS fluorescence, DSC, and NMR, (iii) the ratio of the van't Hoff enthalpy of denaturation and the calorimetric enthalpy obtained from DSC are close to unity, (iv) the kinetics of both unfolding and refolding are monophasic processes (refolding monitored by ANS fluorescence shows a second low-amplitude slow phase; for discussion of this see below), (v) the kinetic data fit a two-state transition as described by eq 4, and (vi), the values for ΔG_{H_2O} and m calculated from the kinetic experiments are closely similar to the values calculated from the equilibrium experiments, Table 1. From these data, and the denaturation profiles as plotted in Figures 4 and 5, the change in heat capacity for the unfolding reaction ΔC_p can be derived from the variation of ΔH_m with temperature afforded by the addition of GdnHCl. The slope of the plot of ΔH_m versus T_m, obtained from CD data shown in Figure 5 (solid line in Figure 12) and from DSC date shown in Figure 4 (dotted line in Figure 12), gives a value of ΔC_p of 6.29 ± 0.43 kJ mol^{-1} K^{-1} and 6.43 ± 0.93 kJ mol^{-1} K^{-1}, respectively. These values are closely similar to that obtained from CD studies for HPr using urea as denaturant (6.23 kJ mol^{-1} K^{-1}; *20*).

The thermodynamic parameters for the folding of HPr from both *E. coli* (this work and ref 20) and *B. subtilis* (*19*) are given in Table 4. The conformational stability of a protein can be expressed in terms of the free energy over a wide range of temperatures, which is described by the Gibbs−Helmholtz relation (eq 3). From this equation, stability curves can be constructed using the parameters for ΔC_p, T_m, and ΔH_m given in Table 4; they are shown in Figure 13. The thermodynamic parameters obtained from DSC and CD in 10 mM phosphate at pH 7.0 used here to study the denaturation of *E. coli* HPr are closely similar but are substantially different from the values reported using urea as denaturant studied by CD (*20*). The temperature of maximum stability (T_s) and the corresponding free energy (ΔG_s) deviate by 6−8 °C and 4−6 kJ mol^{-1}, respectively

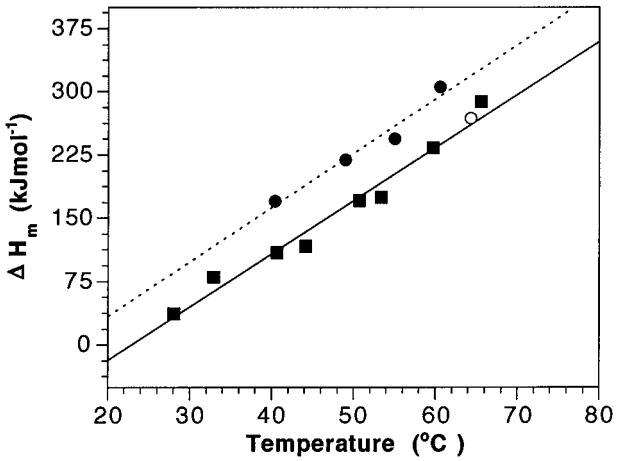

FIGURE 12: Estimation of the heat capacity change upon unfolding from DSC and CD data: Variation of ΔH_m with T_m from the thermal unfolding data in the presence of different concentrations of GdnHCl in 10 mM NaP_i, pH 7.6, using DSC (●, Figure 4B) and in 10 mM NaP_i, pH 7.0, using CD (■, Figure 5B); T_m and the corresponding ΔH_m value obtained from DSC measurements of HPr in 10 mM NaP_i, pH 7.0, in the absence of GdnHCl (Figure 4A, ○). The dotted and solid lines represent the best fit of the data to a linear function with ΔC_p describing the slope of the line, and are 6.4 ± 0.9 and 6.3 ± 0.4 kJ mol^{-1} K^{-1}, respectively.

(Figure 13A). The thermodynamic parameters obtained for *E. coli* HPr in 100 mM NaP_i at pH 7.0 and in 10 mM NaP_i at pH 7.6 are, however, closely similar to those reported by Nicholson and Scholtz (*20*). Small differences in pH and/or phosphate concentrations result in significant changes in the stability. It must be noted that small differences in ΔH_m will result in relative large changes in ΔG at lower temperatures. Overall, the stability of *E. coli* HPr is higher than that of the homologous *B. subtilis* species; although the T_m is ∼9 °C lower than that of *B. subtilis* HPr, the much higher value of ΔH_m reflects a bigger free energy conformational stability at low temperatures as given by the Gibbs−

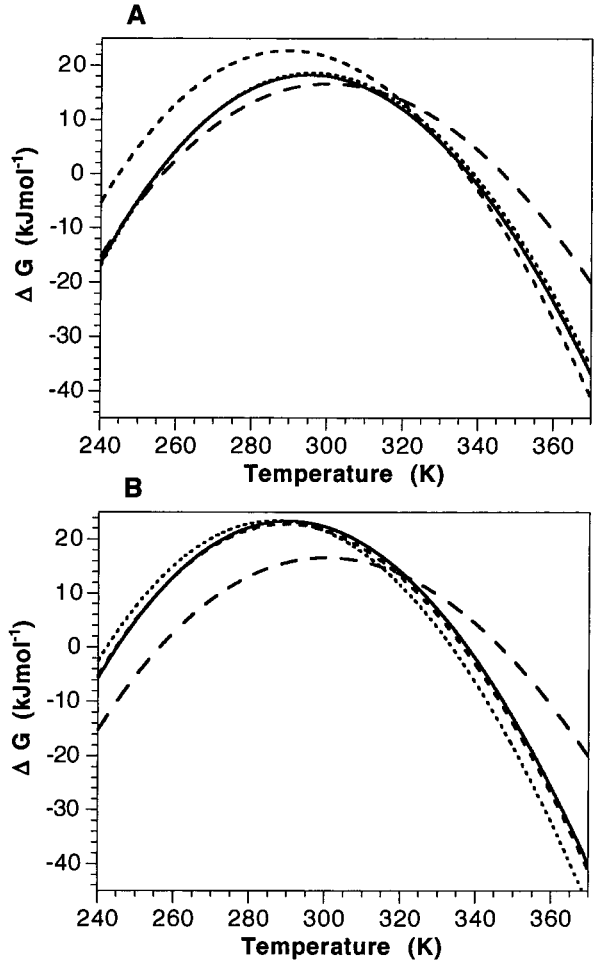

FIGURE 13: Stability curves for *E. coli* and *B. subtilis* HPr obtained from different studies. (A) Stability curves for *E. coli* (short dashed line) and *B. subtilis* (long dashed line) in 10 mM phosphate, pH 7.0, reconstructed from the thermodynamic parameters summarized in Table 4, reported by Nicholson and Scholtz (*20*) and Scholtz (*19*), respectively, together with those under the same conditions from CD (dotted line) and DSC (solid line) measurements reported here using the Gibbs−Helmholtz eq (eq 3). (B) The first two stability curves in A together with those for HPr in 10 mM phosphate at pH 7.6 from DSC (dotted line) experiments and in 100 mM phosphate at pH 7.0 from CD (solid line) experiments.

Helmholtz relationship (eq 3). While experimental values for ΔC_p and m for *B. subtilis* HPr correspond well with those predicted from changes in accessible surface areas (*39*), values for *E. coli* HPr deviate substantially from these relationships. ΔC_p for the latter can be described more adequately by the change in nonpolar and polar accessible surface areas previously described by Murphy and Freire (*40*). The difference in ΔC_p between that of *B. subtilis* and *E. coli* HPr can partially be explained by the differences in heat capacity for their unfolded states based on the amino acid composition (*41*) which are 19.14 and 19.86 kJ mol^{-1} K^{-1} for *B. subtilis* and *E. coli* HPr, respectively. Both ΔC_p and ΔH_m for *E. coli* HPr are relatively high compared to other small globular proteins (*42, 43*). Despite this, we are able to observe cold denaturation in the presence of low concentrations of denaturant, and in the presence of 1.6 M GdnHCl, almost complete unfolding occurs at low temperature.

None of the techniques used to monitor the refolding of HPr from high concentrations of GdnHCl shows any events in the dead-time of the measurements ($\leq$4 ms for the optical spectroscopy methods). The far-UV CD and NMR data show a single well-defined folding step with a rate constant of 1.98 $\pm$ 0.02 s^{-1} at 19.5 °C (far-UV CD), consistent with a two-state refolding reaction as observed for a range of other small proteins (*18*). The ANS fluorescence data show a similar kinetic step, although an overshoot corresponding to an amplitude of ca 20% of the ANS fluorescence associated with the native state. The rate of the recovery phase in this experiment (ca. 0.1 s^{-1}) is similar to that found in other systems for proline isomerisation (*35*), and its activation enthalpy (82.3 kJ mol^{-1}) is in the range expected for such a process (67−84 kJ mol^{-1}; *44*). One explanation of this phenomenon, therefore, is that it arises as a consequence of the transient accumulation of a small population of folded protein molecules with one or both of the two proline residues (Pro11 and Pro18) in the non-native *cis* conformation. A similar overshoot is, however, observed in the dead-time of the fluorescence measurements during the kinetic unfolding of the protein into high concentrations of GdnHCl. Moreover, enhanced ANS fluorescence is observed at low concentrations of GdnHCl in equilibrium unfolding experiments. Neither of these effects is likely to be associated with proline isomerization. It is possible, however, that local conformational heterogeneity under these various conditions results in the population of species with enhanced ANS binding properties; indeed the anomalous behavior of Ala10 and His15 in the equilibrium unfolding experiments monitored by NMR (Figure 2) would be consistent with such heterogeneity.

Both equilibrium and kinetic experiments show, therefore, that HPr behaves as a two-state system in which only native and unfolded states are significantly populated. The native state of a protein is generally assumed to be a single conformation, in contrast to the unfolded state which is an ensemble of different rapidly interconverting conformations (*45*). The transition state for the folding reaction may be visualized as an ensemble of structures located midway between the folded and unfolded state (*46*). Results from experimental work addressing the nature of the transition state ensemble can be rationalized in terms of the energy landscape view of folding (*47*), as well as more conventional descriptions of the folding reaction. While the energy landscape for the folding of a polypeptide chain is complex (*48*), it is useful to model a folding reaction by implying a well-defined transition state. According to the microreversibility principle, the transition state for unfolding will be the same as the transition state for refolding in a two-state process. Studies on the temperature and GdnHCl dependence of unfolding and refolding give thermodynamic information on the nature of this transition state and on its relative exposure to solvent; Figure 14 shows the reaction profiles showing this for HPr.

Both the activation enthalpy for folding, $\Delta H^{\ddagger}$, and the activation entropy for folding, $\Delta S^{\ddagger}$, can also be obtained from the Eyring plot; the values are 86.1 kJ mol^{-1} and 56.0 J mol^{-1} K^{-1}, respectively. The large positive change in enthalpy for refolding is the result of favourable interactions within the polypeptide chain. At 20 °C both the enthalpy and entropy changes upon unfolding are negative (Figure 14A,B), a direct

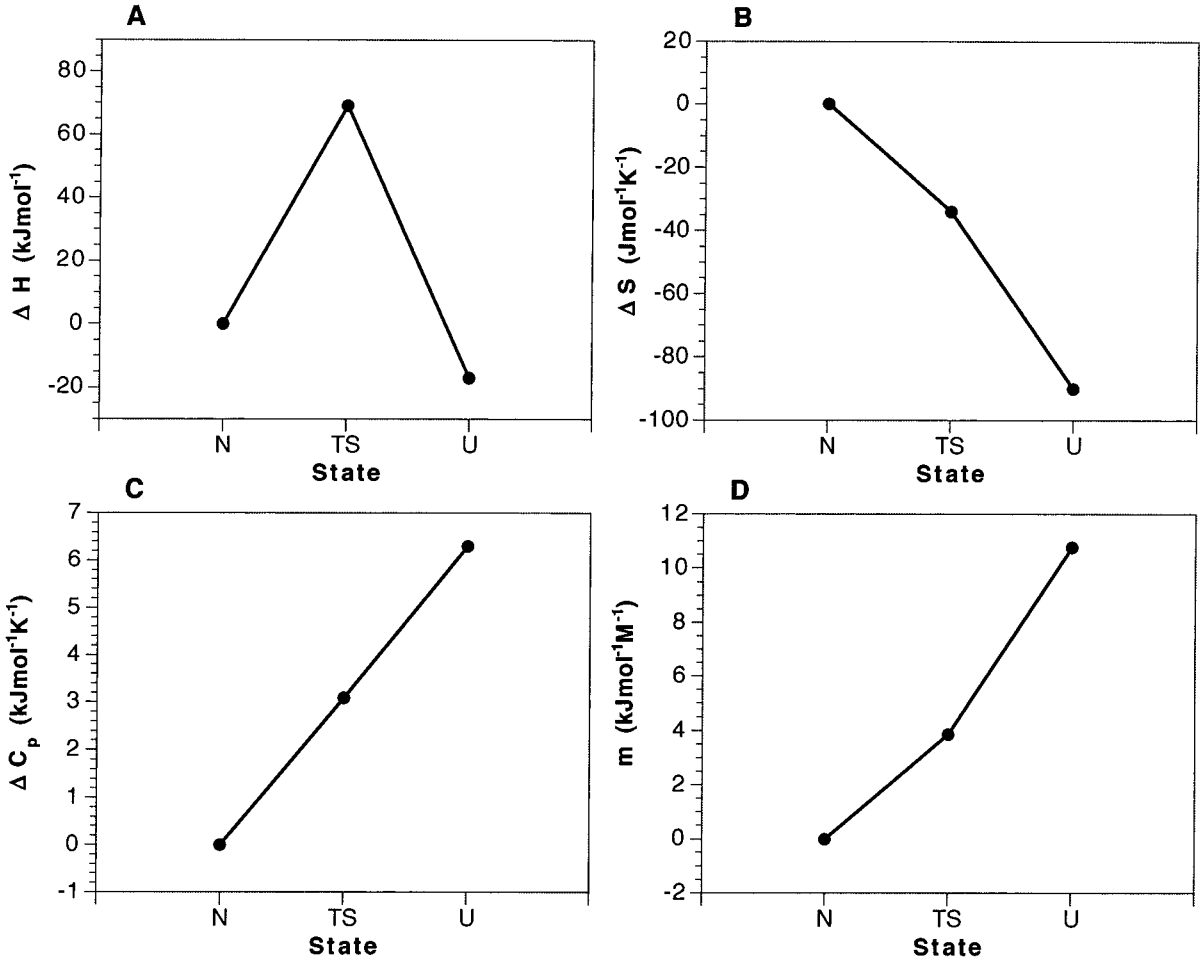

FIGURE 14: Reaction profiles for HPr under native conditions: 0.55 M GdnHCl, 100 mM NaP_i, pH 7.0, 20 °C. The native state (N) is taken as reference point, from which the reaction proceeds through the transition state (TS) to the denatured state (U). (A) Changes in enthalpy; (B) changes in entropy; (C) changes in heat capacity; and (D) changes in *m* values, between the three states.

result of the relative low ΔH_m and high ΔC_p. The entropy of the transition state is between that of the native and the denatured states under these conditions. The positive sign of the entropy change passing from the denatured to the transition state indicates that in the transition state the contribution form the hydrophobic effect outweighs the loss in the conformational entropy of the chain (*38*).

The Eyring plot for the fast refolding phase shows significant curvature (Figure 11B), indicating that the heat capacity change from the denatured state to the transition state is large. The value for this change is -3.22 kJ mol^{-1} K^{-1}, which is 51% of the total heat capacity change between denatured and native states measured from DSC and CD experiments (Figure 14C). Since $\Delta C_p = \Delta C^{\ddagger}_{pu} + \Delta C^{\ddagger}_{pf}$, a similar change in heat capacity change is expected between the native and transition states. Changes in heat capacity reflect changes in the degree of exposure of hydrophobic residues (*30*, *42*). A second measure for the degree of exposure to the solvent is the *m* value which, at equilibrium, is obtained from GdnHCl-induced denaturation curves such as those shown in Figure 3. The solvent accessibility of the transition state is determined by parameter $a^{\ddagger}$ which equals $m_{k_u}/[m_{k_f} + m_{k_u}]$ and describes the change in solvent accessibility upon moving from the native state to the transition state relative to the change upon total unfolding (*49*). From analysis of the rates of refolding and unfolding as a function of the final GdnHCl concentration (Figure 10) we obtain a value for $a^{\ddagger}$ of 0.36 (Figure 14D), which is lower than based on changes in ΔC_p (0.49). Note that ΔC_p is strictly related to the exposure of hydrophobic residues, while the *m* value is related to the exposure of all residues. The solvent accessibility of the transition state of small proteins has been found to vary significantly from 0.14 for the cold-shock protein CspB (*50*) to a value as large as 0.61 for the truncated form of the N-terminal domain of λ-repressor, λ_{6-85} (*51*). There is no clear relationship between the folding rate constant and the compactness of the transition state (*51*). These results do, however, indicate that there is a significant loss in surface area exposed to the solvent between the denatured and transition state and that the exposure of residues decreases progressively to the native state.

The activation energy of refolding (the change in free energy between the denatured and transition states), $\Delta G^{\ddagger}$, obtained from the temperature dependent refolding experiments agrees within experimental error with that obtained from GdnHCl dependent refolding under the same conditions (0.55 M GdnHCl, 100 mM NaP_i, pH 7.0, 20 °C) and are 69.7 and 69.0 kJ mol^{-1} K^{-1}, respectively. At 0 M GdnHCl this value is 65.2 kJ mol^{-1} K^{-1}, similar to the activation energy found for CI2 (63.5 kJ mol^{-1} K^{-1} at 25 °C, 0 M GdnHCl, pH 6.3; *38*).

A more useful parameter to compare the refolding of HPr with that of other, similar sized proteins is the rate constant for refolding in the absence of denaturant, $k_f^{H_2O}$, which is directly proportional to the equilibrium constant between the denatured and transition states. Proteins studied so far include (i) largely helical proteins, e.g., acylcoenzyme A binding protein and related homologous proteins (*52*, 53), the monomeric λ-repressor and a truncated form of it, λ_{6-85} (*51*,*54*), and the B-domain of protein A (*55*), (ii) largely sheet proteins, e.g., the SH3 domain of α-spectrin (*56*), CspB (*50*), and tendamistat (*57*), and (iii) mixed α/β proteins, e.g., CI2 (*38*, *58*), the B domain of the IgG-binding protein G (*59*), the B1 domain of streptococcal protein G (*60*), the activation domain of human procarboxypeptidase A2 (*61*), and arc repressor (*62*). These proteins all have in common that they fold rapidly in the absence of intermediates. Values reported for $k_f^{H_2O}$ obtained under conditions similar to those used here for HPr vary between 4900 s^{-1} for λ_{6-85} (*51*) to 47.8 s^{-1} for CI2 (*58*). The value for HPr (14.9 s^{-1}) extends the range of rates over which two-state folding behavior is found. It shows that proteins smaller than 100 amino acid residues which fold in the absence of detectable intermediates in a two-state manner do not necessarily fold very rapidly.

ACKNOWLEDGMENT

We thank R. ten Hoeve-Duurkens for purifying the protein. We are grateful to A. I. Azuaga and F. Chiti for many helpful discussions.

REFERENCES

1. Dobson, C. M., and Ptytsin, O. B. (1997) *Curr. Opin. Struct. Biol. 7*, 1−2.
2. Plaxco, K. W., and Dobson, C. M. (1996) *Curr. Opin. Struct. Biol. 6*, 630−636.
3. Balbach, J., Forge, V., Van Nuland, N. A. J., Winder, S. L., Hore, P. J., and Dobson, C. M. (1995) *Nat. Struct. Biol. 2*, 865−870.
4. Hoetzli, S. D., and Frieden, C. (1996) *Biochemistry 35*, 16843−16851.
5. Balbach, J., Forge, V., Lau, W. S., Van Nuland, N. A. J., Brew, K., and Dobson, C. M. (1996) *Science 274*, 1161−1163.
6. Postma, P. W., Lengeler, J. W., and Jacobson, G. R. (1993) *Microbiol. Rev. 57*, 543−594.
7. Hammen, P. K., Waygood, E. B., and Klevit, R. E. (1991) *Biochemistry 30*, 11842−11850.
8. Van Nuland, N. A. J., Grötzinger, J., Dijkstra, K., Scheek, R. M., and Robillard, G. T. (1992) *Eur. J. Biochem. 210*, 881−891.
9. Van Nuland, N. A. J., Hangyi I. W., Van Schaik R. C., Berendsen H. J. C., Van Gunsteren, W. F., Scheek, R. M., and Robillard, G. T. (1994) *J. Mol. Biol. 237*, 544−559.
10. Wittekind, M., Rajagopal, P., Baranchini, B. R., Reizer, J., Saier, M. H., Jr., and Klevit, R. E. (1992) *Protein Sci. 1*, 1363−1376.
11. Kalbitzer, H. R. and Hengstenberg, W. (1993) *Eur. J. Biochem. 216*, 205−214.
12. Herzberg, O., Reddy, P., Sutrina, S., Saier, M. H., Reizer, J., and Kapafia, G. (1992) *Proc. Natl. Acad. Sci. U.S.A. 89*, 2499−2503.
13. Jia, Z., Vandonselaar, M., Quail, J. W., and Delbaere, L. T. J. (1993) *Nature 361*, 94−97.
14. Jia, Z., Quail, J. W., Waygood, E. B., and Delbaere, L. T. J. (1993) *J. Biol. Chem. 268*, 22490−22501.
15. Pastore, A., Saudek, V., Ramponi, G., and Williams, R. J. P. (1992) *J. Mol. Biol. 224*, 427−440.
16. Swindells, M. B., Orengo, C. A., Jones, D. T., Pearl, L. H., and Thornton J. M. (1993) *Nature 362*, 299.
17. Liao, D.-I., and Herzberg, O. (1994) *Structure 2*, 1203−1216.
18. Miranker, A. D., and Dobson, C. M. (1996) *Curr. Opin. Struct. Biol. 6*, 31−42.
19. Scholtz, J. M. (1995) *Protein Sci. 4*, 35−43.
20. Nicholson, E. M., and Scholtz, J. M. (1996) *Biochemistry 35*, 11369−11378.
21. Van Nuland, N. A. J., Van Dijk, A. A., Dijkstra, K., Van Hoesel, F. H. J., Scheek, R. M., and Robillard, G. T. (1992) *Eur. J. Biochem. 203*, 483−491.
22. Pace, C. N (1986) *Methods Enzymol. 131*, 266−280.
23. Santoro, M. M., and Bolen, D. W. (1988) *Biochemistry 27*, 8063−8068.
24. Live, D. H., Davis, D. G., Agosta, W. C., and Cowburn, D. (1984) *J. Am. Chem. Soc. 106*, 1939−1941.
25. Redfield, A. G., and Kunz, S. D. (1975) *J. Magn. Reson. 19*, 250−254.
26. Santoro, M. M., and Bolen, D. W. (1992) *Biochemistry 31*, 4901−4907.
27. Pace, C. N., and Tanford, C. (1968) *Biochemistry 7*, 198−208.
28. Robertson, A. D., and Baldwin, R. L. (1991) *Biochemistry 30*, 9907−9914.
29. Agashe, V. R., and Udgaonkar, J. B. (1995) *Biochemistry 34*, 3286−3299.
30. Privalov, P. L. (1979) *Adv. Protein Chem. 33*, 167−241.
31. Dill, K. A., and Shortle, D. (1991) *Annu. Rev. Biochem. 60*, 795−825.
32. Gadian, D. G. (1984) *Nuclear magnetic resonance and its application to living systems*, Clarendon Press, Oxford.
33. Lu, H. (1996) D.Phil. Thesis, University of Oxford, Oxford, England.
34. Sharma, S., Hammen, P. K., Anderson, J. W., Leung, A., Georges, F., Hengstenberg, W., Klevit, R. E., and Waygood, E. B. (1993) *J. Biol. Chem. 268*, 17695−17704.
35. Mayr, L. M., Kiefhaber, T., and Schmid, F. X. (1993) in *Protein Folding: In Vivo and In Vitro* (Cleland, J. L., Ed.) pp 142−155, American Chemical Society, Washington, DC.
36. Chen, Y., Reizer, J., Saier, M. H., Jr., Fairbrother, W. J., and Wright, P. E. (1993) *Biochemistry 32*, 32−37.
37. Van Nuland, N. A. J., Kroon, G. J. A., Dijkstra, K., Wolters, G. K., Scheek, R. M., and Robillard, G. T. (1993) *FEBS Lett. 315*, 11−15.
38. Jackson, S. E., and Fersht, A. R. (1991) *Biochemistry 30*, 10436−10443.
39. Myers, J. K., Pace, C. N., and Scholtz, J. M. (1995) *Protein Sci. 4*, 2138−2148.
40. Murphy, K. P., and Freire, E. (1992) *Adv. Protein Chem. 43*, 313−361.
41. Makathadze, G. I., and Privalov, P. L. (1990) *J. Mol. Biol. 213*, 375−384.
42. Privalov, P. L., and Gill, S. J. (1988) *Adv. Protein Chem. 39*, 191−234.
43. Alexander, P., Fahnestock, S., Lee, T., Orban, J., and Bryan, P. (1992) *Biochemistry 31*, 3597−3603.
44. Brandts, J. F., Halvorson, H. R., and Brennan, M. (1975) *Biochemistry 14*, 4953−4963.
45. Smith, L. J., Fiebig, K. M., Schwalbe, H., and Dobson, C. M. (1996) *Folding Design 5*, R95−R106.
46. Fersht, A. R. (1997) *Curr. Opin. Struct. Biol. 7*, 3−9.
47. Shoemaker, B. A., Wang, J., and Wolynes, P. G. (1997) *Proc. Nat. Acad. Sci. U.S.A. 94*, 777−782.
48. Bryngelson, J. D., Onuchic, J. N., Socci, N. D., and Wolynes, P. G. (1995) *Proteins: Struct. Funct. Genet. 3*, 167−195
49. Tanford, C. (1970) *Adv. Protein Chem. 24*, 1−95.
50. Schindler, T., Herrler, M., Marahiel, M. A., and Schmid, F. X. (1995) *Nat. Struct. Biol. 2*, 663−673.
51. Burton, R. E., Huang, G. S., Daugherty, M. A., Fullbright, P. W., and Oas, T. G. (1996) *J. Mol. Biol. 263*, 311−322.
52. Kragelund, B. B., Robinson, C. V., Knudsen, J. Dobson, C. M., and Poulsen, F. M. (1995) *Biochemistry 34*, 7217−7224.
53. Kragelund, B. B., Højrup, P., Jensen, M. S., Schjerling, C. K., Juul, E., Knudsen, J., and Poulsen, F. M. (1996). *J. Mol. Biol. 256*, 187−200.

54. Huang, G. S. and Oas, T. G. (1995). *Proc. Natl. Acad. Sci. U.S.A. 92*, 6878−6882.
55. Bai, Y., Karimi, A., Dyson, H. J., and Wright, P. E. (1997) *Protein Sci. 6*, 1449−1457.
56. Viguera, A. R., Martínez, J. C., Filimonov, V. V., Mateo, P. L., and Serrano, L. (1994) *Biochemistry 33*, 2142−2150.
57. Schönbrunner, N., Koller, K.-P., and Kiefhaber, T. (1997) *J. Mol. Biol. 268*, 526−538.
58. Jackson, S. E., and Fersht, A. R. (1991) *Biochemistry 30*, 10428−10435.
59. Alexander, P., Orban, J., and Bryan, P. (1992) *Biochemistry 31*, 7243−7248.
60. Kuszewski, J., Clore, G. M., and Gronenborn, A. M. (1994) *Protein Sci. 3*, 1945−1952.
61. Villegas, A., Azuaga, A., Catasús, Ll., Reverter, D., Mateo, P. L., Avilés, F. X., and Serrano, L. (1994) *Biochemistry 33*, 2142−2150.
62. Waldburger, C. D., Jonsson, T., and Sauer, R. T. (1996). *Proc. Natl. Acad. Sci. U.S.A. 93*, 2629−2634.
63. Lee, B., and Richards, F. M. (1971) *J. Mol. Biol. 55*, 379−400.
64. Richards, F. M. (1977) *Annu. Rev. Biophys. Bioeng. 6*, 151−176.
65. Kraulis, P. J. (1991) *J. Appl. Crystallogr. 24*, 946−950.

BI9717946